https://doi.org/10.2352/ISSN.2470-1173.2020.16.AVM-019

Automotive Image Quality Concepts for the next SAE levels: Color Separation and Contrast Detection Probability

Marc Geese, Camera Module Architect at Continental AG in Ulm, Germany

Abstract

In this paper, we present an overview of automotive image quality challenges and link them to the physical properties of image acquisition. This process shows that the detection probability based KPIs are a helpful tool to link image quality to the tasks of the SAE classified supported and automated driving tasks. We develop questions around the challenges of the automotive image quality and show that especially color separation probability (CSP) and contrast detection probability (CDP) are a key enabler to improve the knowhow and overview of the image quality optimization problem. Next we introduce a proposal for color separation probability as a new KPI which is based on the random effects of photon shot noise and the properties of light spectra that cause color metamerism. This allows us to demonstrate the image quality influences related to color at different stages of the image generation pipeline. As a second part we investigated the already presented KPI Contrast Detection Probability and show how it links to different metrics of automotive imaging such as HDR, low light performance and detectivity of an object. As conclusion, this paper summarizes the status of the standardization status within IEEE P2020 of these detection probability based KPIs and outlines the next steps for these work packages.

Introduction

With the recent progress in advanced driver assistance systems the demanded level of automation by the market increase from the current SAE Levels[4] of 2 or 2+ and will demand systems that are characterized as Level 3, 4 or even 5 in the near future. In those higher SAE-Level driving systems, the car itself has to judge critical situations itself and thus its sensory setup needs to produce signals that allow to generate the demanded decisions with high enough probability.

Camera systems will play a major role for these systems as the whole automotive environment and supporting legislation processes are focused on the human visual system. Thus lane markings, traffic signs and even situation judgment will be conducted on the visual data that the human driver would have observed, as the ground truth.

While the standard driving situations like lane keeping, lane changing and automatic emergency braking are already found in series produced cars e.g. [1, 5], these cars do not cover all critical use cases to fulfill SAE Level 3 and above. For example, an automatic braking can be prone to misjudgment if the collision object is not within the currently trained database. Another example could be severe weather situations that disallow to judge the situation with the available sensor setup. However for L3 it is demanded to cover those use cases to a certain extend.

Fig. 1 to 8 show examples of critical use cases gathered from the news media that did occur during 2019. It is therefore likely that a given model of a car will encounter such situations during its service. In this paper we investigate a support structure that helps to indicate if a camera system will be able to fulfill a given use cases.

Figure 1: Example of debris on street with a cardboard box. While a cardboard box could maybe be driven over, their content could be hazardous [6].

Figure 2: Example of debris: A black sofa on the street [7].

Automotive Use Cases: From Scenes and Objects to Color and Contrast

Use Case: Debris on Street

As first example, fig. 1 shows a large cardboard box on a highway [6]. While a pure cardboard box itself could be judged as not harmful, the content inside could be hazardous. Thus it is mandatory to identify such an object correctly.

In the shown example the object differs from the background mainly by its luminance contrast. For machine vision a first guess main feature could be the shape of the object border and the shadows created by the cardboard box. However, these features might change if the illumination conditions change. Summarizing, a general machine vision algorithm might take the a shape surrounded by weak contrast edges into account, plus additionally the high contrast shadows if they are present and fitting the object signature. Consequently, a contrast feature based detection is likely to be used.

Fig. 2 shows a black sofa on the street [7], an object which

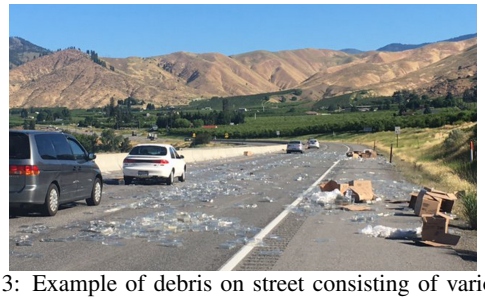

Figure 3: Example of debris on street consisting of various deformed metal and tool parts [8]. A collision needs to be avoided due to tire damage even if the parts are small

Figure 4: In this figure a set of standard white lane markers are shown next to a a set of yellow lane markers [9]. Depending on the context either of the two types of lane markers is the guiding one, and thus both needs to be detected. A contrast detection of the luminance difference between marker and background is necessary as well as a color separation of the yellow against the white marking.

is usually not considered in this context. Compared to the carton from fig.1 a sofa is larger and can easily be detected. A collision needs to be avoided due to the size of the object and the consequences for the car. In daylight the sofa is easy to detect, due to its huge luminance contrast against the street. A machine vision algorithm could again target the large contrast between the low reflectivity sofa against the street background as a mandatory feature for detection. However that contrast is generated by the low reflectivity of the sofa which makes its detection at low light conditions more difficult, especially for black asphalt as street cover.

Fig. 3 shows debris from unknown source, most likely gardening tools, that exist of some metal parts [8]. The difficulty of such use cases is the relative small size of the objects. They need to be detected, but their luminance contrast can be small especially for challenging illumination conditions. However, in this example the occurrence of multiple small objects can help to identify the road as being not drivable.

Depending on the used algorithm, a variety of contrast and luminance based features can be used by the machine vision algorithms. A first guess would again target to identify the contrast changes of the road against the debris and to separate the color of the debris from the color of the road.

Use Case: Lane Markings

Fig. 4 shows an example of dirty and old lane markings [9]. Lane markings usually present a weber contrast of approximately 40%. However if they are dirty or if they show up in counter light situations, it can happen that the contrast diminishes or even

Figure 5: A worn out yellow double line is depicted on a wet road surface [10], that can be detected by machine vision using contrast and color separation features

Figure 6: A typical scene when exiting a parking garage [11]. Many signs and lane markings need to be considered inside and outside the garage to have a full scene understanding. While inside the garage the luminance is low, outside the garage the luminance can be magnitudes higher. Consequently the lane contrast needs to be detected over a large dynamic range.

inverts. In the later case the street appears bright, while the lane marking appears dark. For computer vision tasks the detection of the lanes' contrast against their background is essential and presents a well measurable feature.

In fig. 4 the worn out old yellow lines also need to be considered. Given just the picture it is not possible to tell if these lines are valid and just await renewal, or if they are invalid and await final removal.

Fig. 5 shows another example of worn out lines. Again, depending on the current road context, they might be valid or not. In case of being valid, their low luminance contrast needs to be detected and their color needs to be separated against different colored lines. In the depicted case the lane marking is presenting itself at higher luminance levels due to reflection of white cloudy sky on the wet road.

Use Case: High Dynamic Luminance Range

Fig. 6 shows a situation with a high luminance range also called a HDR scene or High dynamic range scene. The lane markings need to be detected inside and outside the garage and therefore need to be traced over several magnitudes of luminance. A further investigation of such scenes is done in sec. .

Use Case: Persons and Animals

Fig. 7 shows a pedestrian in a not illuminated part of the road [13]. Such situations are more common than one would imagine, as defective street lamps and long hours of darkness during a day

Figure 7: Maybe the most sensitive use case: A pedestrian at night, not well illuminated by the street lamp and thus hard to detect [13]. Despite the manifold geometric features of pedestrians in different positions, the detection of the pedestrian's contrast against its background is a mandatory enabler to perform pedestrian detection.

Figure 8: A horse on the German Autobahn [12]. Animals evolved in a way that they camouflage themselves against the background in many cases. Because a detection of animals is necessary, low contrasts and fine color separation are mandatory for a safe detection.

in certain areas in the world increase the likelihood of such situations.

Pedestrians are usually detected by specially trained machine vision algorithms that need to identify the huge variety of poses and other geometric features that come from different spatial frequencies. However, to enable this, the detection of the contrasts of these features need to achieved by the imaging system with probability required by the algorithms. This means that certain spatial high frequency features need to be detected with a lower probability of around 30% only. While the contrast on the low spatial frequency main body maybe needs to be detected with a 90% probability to achieve the desired performance.

Thus again, the detection probability of contrasts plays a major role to execute the detection tasks at hand, but knowledge of the specific algorithm is mandatory as well to predict the performance of the system.

Fig. 8 shows a horse on a German Autobahn [12]. As animals have evolved to camouflage against their natural background, the horse presents a low contrast against parts of the background. This yields to a detection task for the machine vision algorithms that relies on the detection of low contrasts and fine color separations.

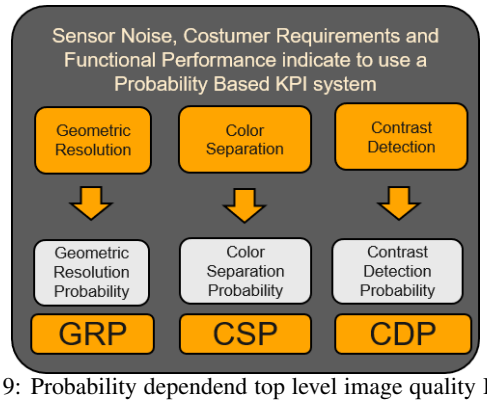

Figure 9: Probability dependend top level image quality KPIs as they are discussed in the IEEE P2020 working group. Interaction between the KPIs is possible and cannot be avoided. For example increasing the spatial frequency of a signal does not only yield to a different GRP but also influences the depending systems CDP and CSP properties

Image Quality Concepts: Top Level Image Quality KPIs

As discussed in the use case analysis, visual image content can usually be described by a combination of the three properties: Geometry, Color and Contrast. To manage these properties a set of three KPIs is developed in the IEEE P2020 working group which are namely: Geometric Resolution Probability (GRP) , Color Separation Probability (CSP) and Contrast Detection Probability (CDP). All of these KPIs are chosen to be probability based KPIs as the imaging process contains various random and static noise sources.

Geometry features are extracted by the imaging system via its geometric resolution. We propose to measure the geometric resolution by the geometric resolution probability which takes random processes like shifts of the object versus the imagers' light sensor grid into account.

Color features shall target to separate different color to each other. A prominent use case for color separation are traffic lights with their color green, yellow and red. Also the color detection underlies random processes, that arise from noise in the imaging chain but as well from the property of metamerism of certain light spectra. The later case can cause that two different traffic lights that appear to the human observer as red colored, are perceived by a camera as different colors because they emit different spectra. This difference can for example be fonded in the difference between tungsten light sources and LED light sources. In such cases the color separation of an imaging system has a reduced **color separation probability (CSP)**, depending on the lights' spectra.

For contrast detection, especially at low light, even the photon flux exhibits Poisson noise properties and thus contrast detection depends naturally on the intensity level at which the contrast is presented to the system. Further the electronic noise increases with temperature and can also be dominant for some use cases. Consequently a systems' **Contrast Detection Probability (CDP) [17, 18]** has many dependencies that have to be considered given the intended use-cases of the system. CDP is currently prepared as a draft in the IEEE P2020 working group.

Fig. 9 shows the just introduced three top level probability based image quality KPIs. These KPIs are not orthogonal. For

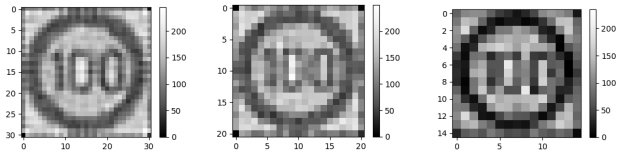

(a) (b) (c)

Figure 10: A noisy image 10a is scaled down which increases the contrast detection probability due to the averaging effect (see 10b). However, scaling down too much destroys important geometric features (10c)

example increasing the spatial frequency of a signal does not only yield to a different GRP for this frequency but also influences the systems CDP and CSP properties that depend on these spatial frequencies.

Fig. 10 shows an example of how the KPIs interact. A noisy signal from a high resolution image whose is consequently scaled down. As one effect the signal to noise ratio increases due to the averaging effect, which consequently leads to an increase in CDP. On the downside however the geometric resolution decreases until some demanded features like the separation between the "1" and the "0" cannot be executed any more. Thus a balance between the geometric resolution and contrast detection needs to be found which allows to fulfill the detection task.

A theoretical approach to find an indication for the right balance between the KPIs can be derived by the detectivity threshold presented by Jenkin and Kane [14, 15]. However, if a specific algorithm shall be analyzed its requirements against the relevant KPIs have to be known. Similar to the well known signal to noise ratio (SNR), a flat field analysis of CDP and CSP helps to give a first indication of the system behavior.

System Architecture

The image acquisition process takes place by an imaging chain as depicted in fig. 11. The objects in the scene emit a signal, which is then transferred through the atmosphere onto the windshield or protection glass. By passing the windshield first distortions and artifacts are introduced into the signal. Next the optics project an image of the objects onto the image sensor surface. The imager transforms the light signal from photons into digital numbers and finally the image signal processing (ISP) reconstructs an image which is as close to the original object as possible. The result is then stored into a digital memory.

Having described this level of the imaging chain, a deeper model can be derived if more knowledge of its building blocks is present. Especially for optics, imager and ISP, a further decomposition is necessary to understand all the introduced effects.

On the higher level, the described building blocks can be considered as components of coarser systems like: A camera module consisting of Optics and Imager, or an ADAS camera, consisting of Optics, Imager and ISP. Considering the next broader level, the ADAS camera is part of a car or one of its subsystems. The car itself is part of the Self-Driving-Car-System, which could also include parts of the environment.

Color Separation Probability and the Imaging Chain

As mentioned in the KPI discussion, color separation probability shall be evaluated along the imaging chain introduced in fig. 11.

For color, to execute this, the emitted spectra of the use-case relevant objects need to be captured. After that, it is possible to calculate the human color impression by color theory from the CIE [19]. Fig.12 shows pictures from a measurement campaign, using a JETI spectroradiometer 1511 [2] to obtain emitted spectra from various automotive use cases.

The recorded spectra only cover a small subset of the infinity of possible spectra that can occur during driving situations. Further we need to consider metamerism, where two different spectra yield to the same color impression, but could lead to different color reconstruction on the camera. The resulting task is therefore to create an arbitrary amount of different spectra for any chosen chromaticity point, while fulfilling the side condition that these spectra shall be similar to the spectra measured for the demanded use cases.

Fig. 13 shows different spectra that create the same visual impression for humans but could lead to different color reconstruction when observed with a camera. Considering the imaging chain from fig. 11, the following different aspects are known to influence color reconstruction the most: IR- and UV-filters of the Optics, the choice of the color filter array of the imager and the configuration and tuning of the image signal processing.

A spectra generation method

Fig. 14, 15 and 16 show a mathematical optimization method that executes the above demanded spectra generation.

Fig. 14 sketches the basic idea of spectra generation by a linear combining of a set of base spectra B. However, the measured base spectra might not be able to reach all points of the chromaticity plane. To fix this random spectra and delta-peak spectra A are added into the combination matrix. Multiplying the spectra matrix (AB) with a set of weights w, results in a target spectra S. This spectra can be multiplied to the CIE's color sensitivity curves $(x(\lambda)y(\lambda)z(\lambda))^T$, resulting in its (X,Y,Z) coordinates, that can be transferred into the chromaticity plane.

The described system of equations can be solved for its non-negative solution to obtain a set of weights w that allow a spectra generation. However, only a unique set of weights can be found this way.

As multiple solutions to the equation from fig. 14 exist, the method is refined in a way that samples the solution space equally. To execute this the base spectra matrix is multiplied onto the sensitivity curves, resulting in a core matrix for the given problem. When multiplying the core matrix with the weight vector W, the first three rows of the result in the targeted XYZ values. A diagonal matrix of penalties for each base spectra is appended where the measured spectra are given a penalty of 1 while the additional random and peak spectra are given higher penalties. On the other side of the equation, the target XYZ values are extended by a randomly chosen set of initialized target weights values T. The random selection guarantees to sample the solution space of the original equation adequately. The target value for the random extra spectra is set to 0 as these shall be used in cases were the goal of XYZ cannot be reached with sufficient accuracy.

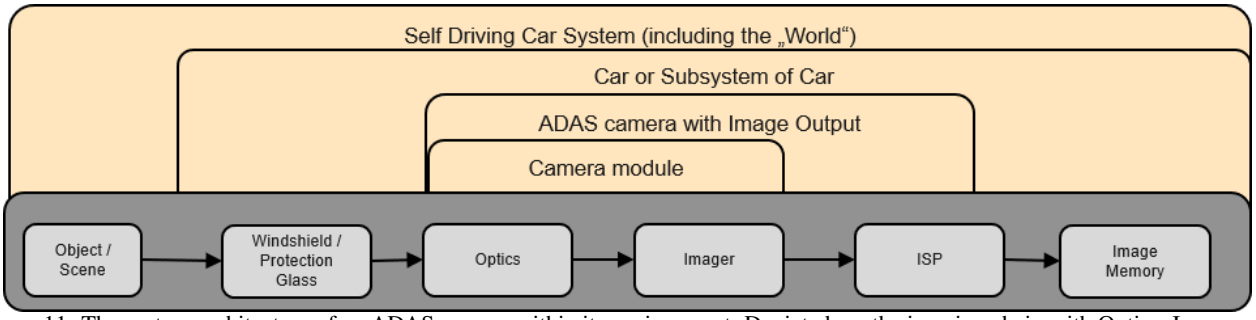

Figure 11: The system architecture of an ADAS camera within its environment. Depicted are the imaging chain with Optics, Imager and ISP as part of the camera module and different (sub-) system borders.

Figure 12: A measurement campaign with a JETI spectroradiometer 1511 [2] to obtain a set of typical spectra for automotive use cases.

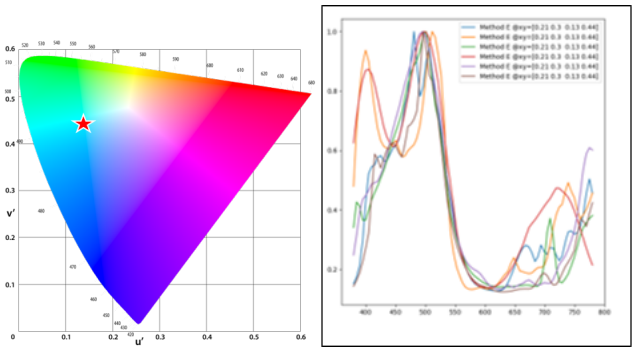

(a) (b)

Figure 13: Fig. 13a shows the CIE Luv color space's chromaticity plane (u,v) a marker at a blueish-green chromaticity coordinate. Fig. 13a shows a set of different metamerism spectra that all yield to the same color impression for humans of the marker. However, the spectra have different peaks, and thus could lead to different color reproductions if viewed by a camera system.

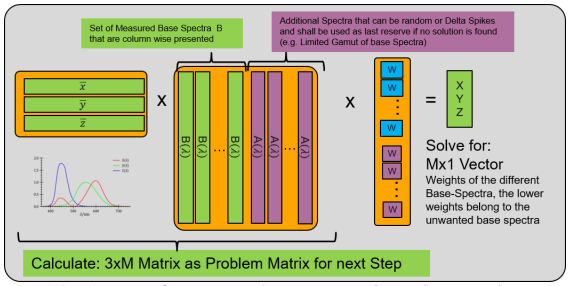

Figure 14: A set of measured spectra B is written column wise next to a set of gamut expanding random spectra. The matrix is multiplied with the CIE color sensitivity curves and the resulting matrix can be multiplied with set of weights for the base-spectra matrix, resulting in a color coordinate in XYZ coordinates. Only non-negative solutions are accepted.

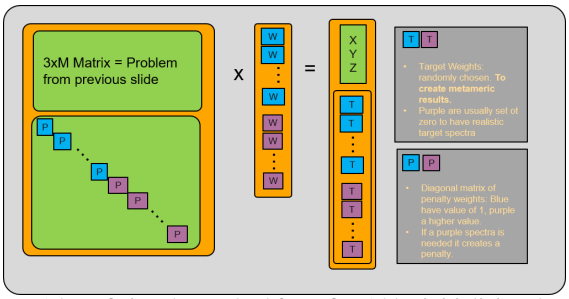

Figure 15: Refining the method from fig. 14 by initializing the optimization problem with a random target combination of the base spectra T and by penalizing the random and delta peak spectra. Again for each initialization the non-negative solutions results in the weights to create a spectra according to fig. 16

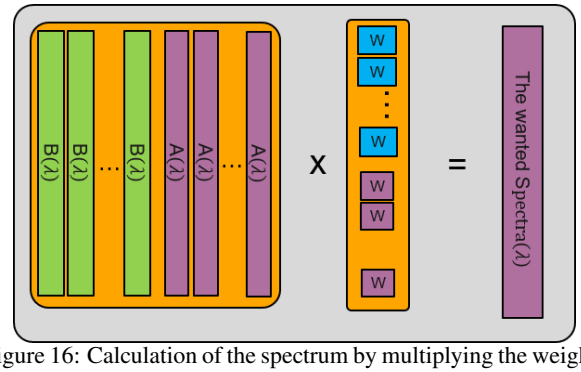

Figure 16: Calculation of the spectrum by multiplying the weights vector from fig. 15 with the matrix of measured base spectra and penalized, random gamut extending spectra.

To obtain several metamerism spectra the procedure is repeated with different initializations. However, in certain situations it is not possible to obtain a solution, for example if the base spectra cover only a limited gamut, which can be caused by a limited or incomplete set of measurements. In such cases the penalty for the artificial random spectra can be lowered. This penalty lowering process can be repeated until a solution is found. Finally fig. 16 illustrates how the spectra can then be calculated from the found weights.

Color Separation Probability

Fig. 17 shows the resulting chromaticity errors for two set of metamerism spectra. To get a better overview of the performance of a camera setup, fig. 18 shows different plots of the mean absolute chromaticity error, which is equivalent to the radius of the

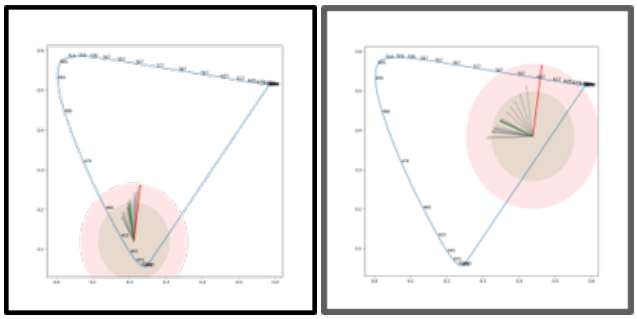

(a) (b)

Figure 17: Fig. 17a and 17b show the resulting delta chromaticity errors for two set of metamerism spectra. The gray errors show the individual errors, the green arrow shows the mean deviation and the red arrow the maximum deviation. The red circle shows the maximum absolute deviation and the green circle shows the mean absolute deviation.

green circle in 17.

Here especially the best found solution is shown in fig. 18a , which could be generated by simulating a 4 channel CFA with the colors: Cyan, Magenta, Yellow and Clear. The reconstruction is generated by an optimized support vector machine learning. Fig. 18b shows a standard RGB 3-channel CFA and fig. 18c shows the difference for the same RGB CFA but this time evaluated by a $3x3$ color correction matrix that was optimized to generate the lowest mean error.

Fig. 18d shows a 3-channel R**C**B CFA which is usually used to optimize low light performance. Here the color reconstruction is again realized by an optimized $3x3$ color correction matrix. It can directly be observed that the RCB CFA has a disadvantage in the red-yellow chromaticity area when compared to the RGB CFA.

However this drawback is not caused by the CFAs capabilities but rather by the used color reconstruction method. To prove this, we use in fig. 18e again the multi feature support vector machine to reconstruct the color. We can observe that especially in the yellow-red area of the chromaticity plane, the RCB CFA delivers its highest color accuracy.

The results shown in fig. 18 do not show actual hardware implementations and different results and conclusions are to be expected if the optimizations are focused on certain regions of the chromaticity plane with higher priority. Another approach could be to consider the maximum deviation as optimization target instead of the mean deviation.

This result can also be used to conclude the above discussion of the influences the different KPIs have on each other. In the given examples an improved Color Separation Probability is achieved with a 4-channel CFA. However, such a CFA also limits the geometric resolution compared to an RCCB color filter array which can utilize its two C-filtered light sensors to improve its geometric resolution and contrast detection probability in the obtained signals.

As a visual result, two different ISP tunings out of the same raw data is shown in fig. 19. Here fig. 19a shows the results corresponding to a tuning similar to fig. 18d by a casual optimized 3x3 color reconstruction. Fig. 19b then shows results that are obtained with an ISP tuning that considers the physics of the RCB CFA. It can be clearly seen that the behavior that we expect from the chromaticity error maps in fig. 18d and 18e transfers into the color separation of the red and yellow traffic signs in fig. 19a and 19b. Consequently the red and yellow colors can be separated from each other in fig. 19b. While the task of color separation solved in the shown results, an improved tuning can yield to better accuracy of the red colors.

We propose to base the **Color Separation Probability (CSP)** KPI with help of the presented method onto a chromaticity error maps in which the color could be generated as it follows: A spectra shall be counted as 1 if it falls inside an accepted requirement of a local chromaticity deviation and as 0 if it falls outside. The ratio of hit and miss could then be considered as the CSP for the given chromaticity point.

Contrast Detection Probability use Case Analysis

Having discussed color and geometric features in images, the detection of contrasts is now revisited by using the Contrast Detection Probability introduced in [17] and [18]. To estimate appearing contrasts of real world objects a calibrated measurement of the use cases is necessary. We measured automotive use cases with a Radiant Luminance Camera [3].

Fig. 20a shows a use-case of a crossroad with bright traffic light of $\approx 5000\frac{cd}{m^2}$. A female pedestrian exhibits a good visible weber contrast of approximately 100% and a lane with 25% weber contrast:

$$K_{\text{Weber}}(\text{pedestrian body}) = \frac{16\frac{cd}{m^2}}{8\frac{cd}{m^2}} - 1 = 100\% \quad (1)$$

$$K_{\text{Weber}}(\text{Lane}) = \frac{100\frac{cd}{m^2}}{80\frac{cd}{m^2}} - 1 = 25\% \quad (2)$$

Please note that depending on the illumination condition, the emitted contrast differs from the reflectance contrast that would be measured in laboratory setups. Also different illumination conditions may change and reduce the observed contrasts drastically, thus a validation of the assumptions about the needed contrast detection probability has to be executed thoroughly.

Fig. 20b shows a scene inside a tunnel with a luminance emitted from the walls of about $10\frac{cd}{m^2}$ to $20\frac{cd}{m^2}$. The lanes exhibit still a contrast of 20% to 40% weber contrast depending on their position and dirt level.

Mapping Use Cases into a CDP field

With the presented method we can now place the gathered know-how about the use-cases into a measured CDP field. In fig. 21 we show a laboratory measured CDP field and fig. 22 shows an approximate mapping of the initially discussed use cases. Please note that the shown CDP field exhibits the pixel to pixel CDP for an output image at a given resolution.

Similar to SNR values, also CDP can be improved by binning or scaling the output, which however creates a negative influence on the geometric detection as discussed above. With the pixel to pixel data and assuming that the noise data is uncorrelated, the CDP after scaling could also be modeled.

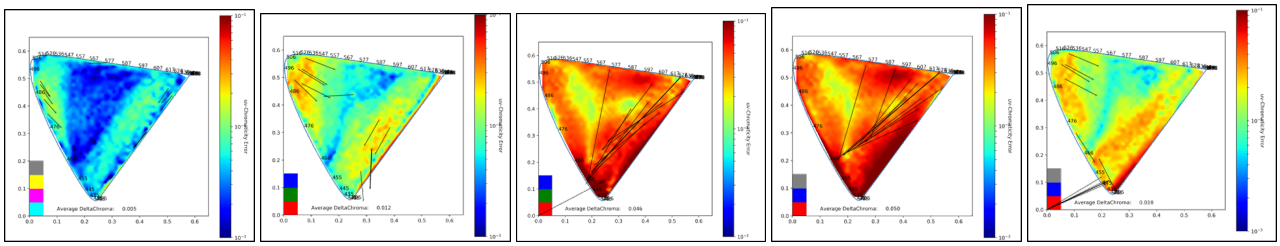

(a) (b) (c) (d) (e)

Figure 18: Different mean chromaticity errors as color map in the chromaticity plane. Fig. 18a shows the best result of the conducted evaluation which is a 4-channel CFA of Cyan, Magenta, Yellow and clear, processed with an optimized machine learning color reconstruction. Fig. 18b shows the RGB CFA processed with an optimized machine learning color reconstruction and fig. 18c shows a color reconstruction with a typical 3x3 color reconstruction matrix. Fig. 18d shows as direct comparison the RCB CFA with a typical 3x3 Color Reconstruction Matrix, which gives higher errors in the region of saturated red and yellow colors.Finally fig. 18e shows the RCB CFA with an optimized machine learning color reconstruction which improves the color deficit in the red-yellow region and closes in towards RGB result from fig. 18b.

(a)

(b)

Figure 19: Fig. 19a shows a picture where the red and yellow traffic signs can not be separated by their color, however a better trained ISP in fig. 19b allows the color separation between yellow and red.

Linking High Dynamic Range KPIs to CDP

Another view on a CDP field (fig. 21) links the Dynamic Range KPIs to CDP. Dynamic Range has been defined e.g. in EMVA1288 [16] and is currently under consideration for IEEE P2020 with an extension that covers modern High Dynamic Range cameras. A high dynamic range, or in other words: a luminance variation over several magnitudes is a very common use case in automotive camera applications. Fig. 23 shows a typical scene with wet road surfaces, captured against the light and including shadows. It has been captured several times over a day with different illumination conditions. Fig. 24 shows the scene with no direct sunlight, as the sun is covered by clouds and fig. 25 shows the same scene with direct sunlight hitting the wet road surface.

The luminance level in the left hand side of this image can be linked to the task of detecting a pedestrian or a lane marking in the shadows next to a passenger car. This luminance level stays in the area of below $500\,\frac{cd}{m^2}$ in both cases, just the color code changes in the two captures (fig. 24 and fig. 25).

The road surface on the other hand changes its luminance level from $10^4\,\frac{cd}{m^2}$ to $2\cdot10^5\,\frac{cd}{m^2}$. Considering lane marker detection, depending on the illumination angle and lane marker reflectance properties, even in this high luminance conditions, the contrast

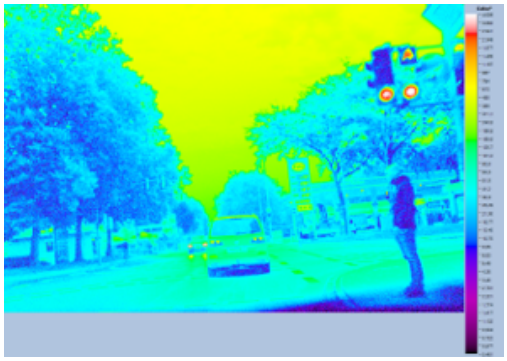

(a)

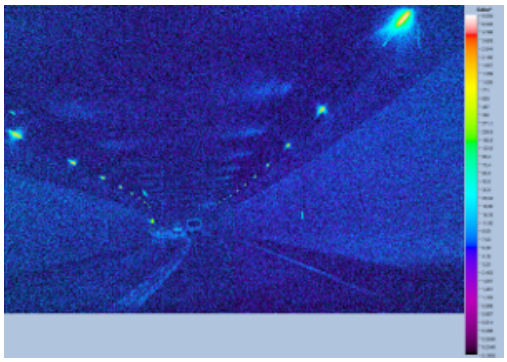

(b)

Figure 20: Classifying use cases for contrast detection analysis by using a Radiant Luminance Camera [3], which produced the measurements in fig. 20a and 20b. Fig. 20a exhibits a bright traffic light of $5000\,\frac{cd}{m^2}$, a pedestrian with 100% Weber contrast and a lane with 25% weber contrast. The tunnel exhibits lanes with contrasts of 20% to 40% at an luminance level of $5\,\frac{cd}{m^2}$ to $10\,\frac{cd}{m^2}$

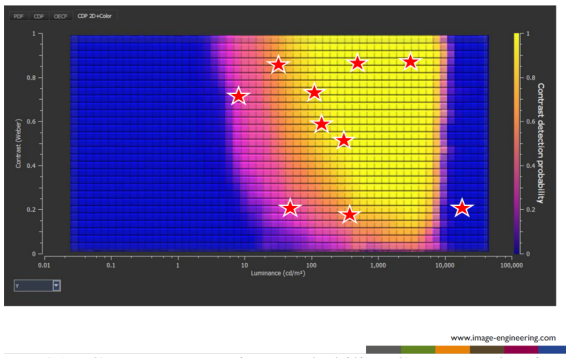

Figure 21: Contrast Detection Probability CDP over luminance and contrast. The color code represents the contrast detection for pixel to pixel CDP of the output image. The stars mark some of the above discussed use cases (see fig. 22 for details.)

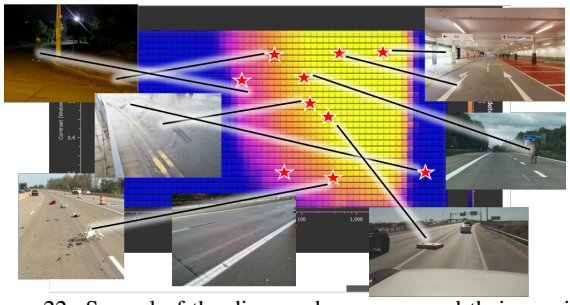

Figure 22: Several of the discussed use cases and their requirement for contrast detection probability mapped into the CDP field from fig. 21.

between road and lane markings resides in the range of 25% or below.

Summarizing just these two use cases, a luminance range of $5 \cdot 10^2 \frac{cd}{m^2}$ and $2 \cdot 10^5 \frac{cd}{m^2}$ leads to a dynamic range of $52dB$:

$$\mathrm{DR[dB]} = 20 \cdot \log \left(\frac{2 \cdot 10^5 \frac{cd}{m^2}}{5 \cdot 10^2 \frac{cd}{m^2}} \right) = 52\mathrm{dB} \tag{3}$$

The calculation can easily extend to higher dynamic ranges if the low light areas become darker, as an entrance into a tunnel or a garage. Considering for example $10 \frac{cd}{m^2}$ for the shadow part and $10^6 \frac{cd}{m^2}$ for the bright part leads to $92dB$. However, this seems like a feasible target for a typical $120dB$ dynamic range sensor.

But the current dynamic range reporting scheme considers usually an SNR1 value as starting reference for HDR measurements (e.g [16]). With the above discussed use cases we know that the detection of weber contrasts of lanes with $K_{\mathrm{weber}} \approx 20\%$ is a typical ADAS task. Consequently, the detection task and the absolute luminance values in which the demanded performance is required have to be analyzed.

In fig. 26 we show how a contrast detection probability based dynamic range value changes for the different CDP requirements for the same camera setup in the following ways:

$$DR = 30\mathrm{dB} \quad C_{20\%}DP \geq 50\% \tag{4}$$

$$DR = 60\mathrm{dB} \quad C_{70\%}DP \geq 20\% \tag{5}$$

$$DR = 40\mathrm{dB} \quad C_{90\%}DP \geq 50\% \tag{6}$$

The discussed camera however could have reported a different SNR1 based HDR capability, but produces only $30dB$ if it

Figure 23: Picture of a typical high dynamic range scene, captured in two different illumination conditions (fig. 24 and 25). Objects of interest could occur in the shadows in the left hand side of the image as well as on the wet street in the center of the image, where high luminance values are reached. A lane marking for 25% weber contrast shall be traced throughout this luminance range.

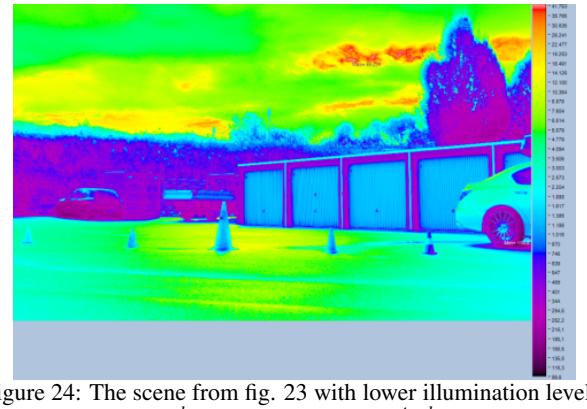

Figure 24: The scene from fig. 23 with lower illumination levels, reaching from $500 \frac{cd}{m^2}$ in the shadows to $10^4 \frac{cd}{m^2}$ on the wet street surface, spreading over $32dB$ of dynamic range

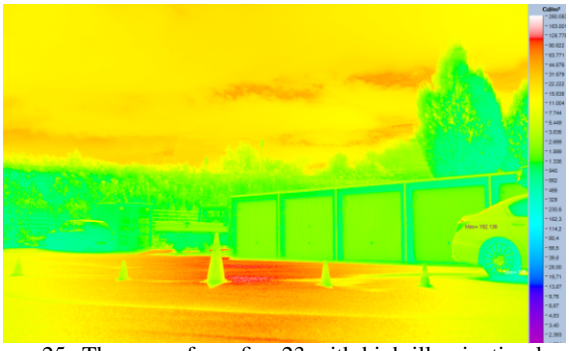

Figure 25: The scene from fig. 23 with high illumination levels, reaching from $500 \frac{cd}{m^2}$ in the shadows to $2 \cdot 10^5 \frac{cd}{m^2}$ on the wet street surface, spreading over $52dB$ of dynamic range

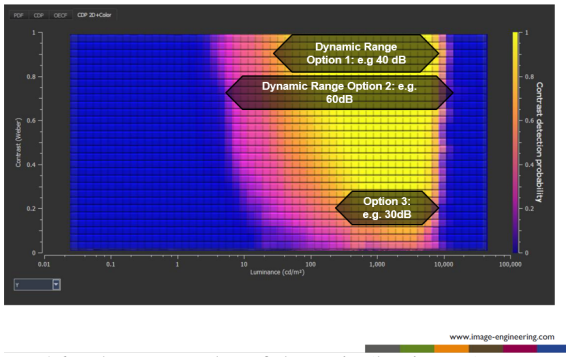

Figure 26: Three examples of dynamic (luminance) ranges that can be reached with a camera when different contrast detection probability goals are considered. The dynamic ranges vary from 30dB for low contrasts to 60dB for high contrasts each with low contrast detection probability. A 40dB dynamic range is reached for high contrasts and high detection probability. These DR-values differ from the ones reported by SNR1 based methods [16]

comes to the detection of small contrasts in a pixel to pixel comparison. Thus we recommend to show a CDP analysis when asked if the HDR capability of a given camera system fits the required use cases.

Conclusions and Summary

In this paper we started with a discussion about automotive imaging use cases and elaborated how and why image quality will become more and more important when the next SAE-levels for autonomous driving are reached. We proposed a set of three probability based KPIs: Geometric Resolution Probability, Color Separation Probability and Contrast Detection Probability. The current status of these KPIs and their interactions has been discussed.

For Color Separation we proposed a heat map of chromaticity errors and reflected the currently ongoing discussions in IEEE P2020 towards a definition of Color Separation Probability (CSP) as a new KPI. To facilitate the color evaluations we developed a method for generation of metamerism spectra that are derived based on real world measurements. We then revisited Contrast Detection Probability (CDP) and linked it to the existing dynamic range KPIs and the above discussed use cases.

Especially the interaction between geometric resolution, the objects detectivity and contrast detection probability has been investigated. As next steps, the IEEE P2020 working group will continue with the development of the Geometric Resolution Probability KPI and finalize the discussions about the standardization of measurements for CSP and CDP.

Acknowledgments

The author wants to thank Image Engineering GmbH & Co. KG for providing and executing the CDP measurements.

References

[1] Daimler AG on available ADAS systems: https://www.daimler.com/innovation/specials/chronologie-der-assistenzsysteme.html, visited 01/2020.

[2] Jeti, VIS Spectroradiometer 1511, https://www.jeti.com/, visited 01/2020.

[3] ProMetric I, Imaging Colorimeters: https://www.radiantvisionsystems.com/, visited 01/2020.

[4] Taxonomy and Definitions for Terms Related to On-Road Motor Vehicle Automated Driving Systems, https://www.sae.org/standards/content/j3016_201401/

[5] https://www.volkswagen-newsroom.com/, visited 01/2020.

[6] https://cbsaustin.com/news/local/debris-on-texas-highways-cause-hundreds-of-crashes-every-year

[7] https://aaafoundation.org/prevalence-motor-vehicle-crashes-involving-road-debris-united-states-2011-2014/

[8] https://www.tribpub.com/gdpr/chicagotribune.com/

[9] http://www.stim.cz/images/photos/1438864635jihlava-2.jpg

[10] https://www.surfprep.co.uk/images/new/lines/line-4.jpg

[11] https://www.meonuk.com/facility-and-car-park-line-marking

[12] https://www.presseportal.de/blaulicht/pm/59460/4317796

[13] https://www.mycoastnow.com/wp-content/uploads/2016/10/pedestrian-at-night.jpg

[14] R. Jenkin and P. Kane, Fundamental imaging system analysis for autonomous vehicles, (https://doi.org/10.2352/ISSN.2470-1173.2018.17.AVM-105)

[15] Kane, Signal Detection Theory and Automotive Imaging (https://doi.org/10.2352/ISSN.2470-1173.2018.17.AVM-148)

[16] Release 3.1, https://www.emva.org/standards-technology/emva-1288/

[17] Geese and Seger: Detection Probabilities: Performance Prediction for Sensors of Autonomous Vehicles (https://doi.org/10.2352/ISSN.2470-1173.2018.17.AVM-148)https://doi.org/10.2352/ISSN.2470-1173.2019.15.AVM-030)

[18] Artmann, Geese and Gde: Contrast Detection Probability - Implementation and use cases (https://doi.org/10.2352/ISSN.2470-1173.2019.15.AVM-030)

[19] The International Commission on Illumination (http://cie.co.at/) in ISO 11664 part 1

Author Biography

Marc Geese received a Diploma in applied physics from Frankfurt University, an MPhil in Electrical Engineering from University of Manchester and a PhD in Physics from Heidelberg University. His research focused on Complex Systems and Neural Networks applied to Image Processing tasks, Vision Chips and Computer Vision Algorithms. In his professional work he spend more than ten years in the field of video based ADAS Systems working for Robert Bosch GmbH and Continental AG. In his role as Camera Module Architect his interest is in automotive image quality is supplemented by serving as a subgroup leader in the IEEE P2020 standardization effort.

JOIN US AT THE NEXT EI!

IS&T International Symposium on

Electronic Imaging

SCIENCE AND TECHNOLOGY

Imaging across applications . . . Where industry and academia meet!

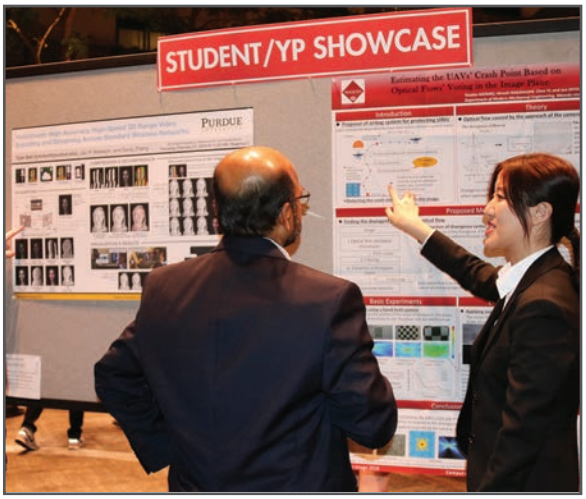

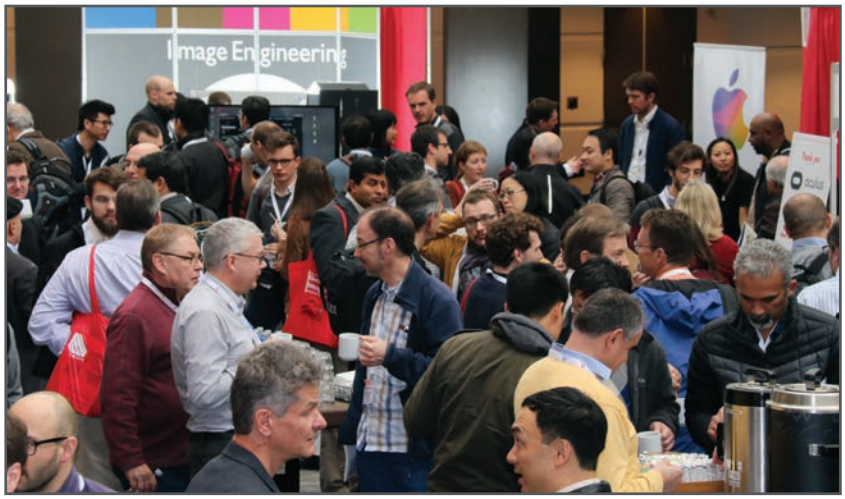

• SHORT COURSES • EXHIBITS • DEMONSTRATION SESSION • PLENARY TALKS •
• INTERACTIVE PAPER SESSION • SPECIAL EVENTS • TECHNICAL SESSIONS •

www.electronicimaging.org

IS&T
imaging.org